Possibility of the simultaneous occurrence of potential minima along two crystallographic directions in an octahedral potential

G. K. Pandey, K. L. Pandey, M. Massey, and Raj Kumar
Department of Physics, University of Allahabad, Allahabad 211 002, Uttar Pradesh, India
(Received 8 November 1985)

It is demonstrated that within the framework of a two-parameter octahedral potential for a dipolar impurity in solid-state matrices, it is possible for the impurity to possess minimum-energy orientational configurations in two crystallographic directions simultaneously. The implication of this conclusion on the possible explanation of certain unexpected results for the NaBr:F^- and RbCl:CN^- systems is discussed.

I. INTRODUCTION

Diatomic and off-centered monatomic impurities in crystals with octahedral symmetry have recently attracted considerable attention. In the limit of infinite potential barriers, these impurities align themselves along certain preferred crystallographic directions. For finite potential barriers, however, they tunnel between the equilibrium orientational configurations, resulting in interesting electrical, thermal, and optical properties. The tunneling splitting of the ground-state level, and the related properties of the system mentioned above, depend critically on the actual minimum-energy orientational configuration of the impurity, apart from certain other parameters such as the height of the potential barrier, the amount of off-center displacement, etc. The simplest form of the octahedral potential for the angular motion of the diatomic impurity in solid-state matrices was first presented by Devonshire[1] and is given by

$$V(\theta,\phi)=-\tfrac{5}{2}K\left[\frac{x^4+y^4+z^4}{r^4}\right], \tag{1}$$

where $x/r=\sin\theta\cos\phi$, $y/r=\sin\theta\sin\phi$, and $z/r=\cos\theta$. Many experimental results for systems such as OH^- and CN^- ions in alkali halide matrices[2,3] and HCl, HBr, etc. Impurities in rare-gas matrices[4,5] have been successfully interpreted in terms of this one-parameter Devonshire potential. It was an easy job to show that for this potential the minimum-energy orientational configuration for the impurity is along one or another of the six ⟨100⟩ directions if K is positive, and along one of the eight ⟨111⟩ directions if K is negative. A ⟨110⟩ minimum-energy configuration was not possible within the framework of the Devonshire potential.

Many recent experimental results on systems such as RbCl:CN^-, KI:OH^-, NaBr:F^-, etc. show strong evidence for the ⟨110⟩ equilibrium orientational configuration for these impurity systems. The Devonshire potential, in fact, retains only the first significant term (the $L=4$ term) in the expansion of the octahedral potential in terms of the spherical harmonics. To make room for the ⟨110⟩ configuration, the next term (the $L=6$ term) was added to make the two-parameter octahedral potential

$$\begin{aligned}V(\theta,\phi)=&-\tfrac{5}{2}K\left[\frac{x^4+y^4+z^4}{r^4}\right]\\&+\tfrac{1}{2}K'\left[180\frac{x^2y^2z^2}{r^6}-\frac{15}{r^6}(x^2y^4+x^2z^4+y^2x^4\right.\\&+y^2z^4+z^2x^4+z^2y^4)\\&\left.+\frac{2}{r^6}(x^6+y^6+z^6)\right].\end{aligned} \tag{2}$$

It was concluded in a previous communication that if $(10/21)<(K'/K)<(-20/189)$, a ⟨110⟩ equilibrium orientational configuration is physically possible.[6,7] This conclusion was also subscribed to later on by Beyeler,[8] who obtained the condition for the ⟨110⟩ potential minima to occur as $26°<\phi<173°$, where $\phi=\tan^{-1}(K'/K)$. Beyeler deduced conditions for other (viz., ⟨100⟩ and ⟨111⟩) equilibrium orientations also in this two-parameter potential, to which we do not fully subscribe. Specifically speaking, Beyeler's conclusion is that for a particular set of values of K and K', any one of the three—⟨100⟩, ⟨111⟩, ⟨110⟩—equilibrium configurations is possible. We have studied the maxima-minima properties of this two-parameter potential in detail and have concluded that there do exist certain sets of values of K and K' for which it is possible to get simultaneous potential minima along either the ⟨111⟩ and ⟨110⟩ directions or the ⟨111⟩ and ⟨100⟩ directions. A simultaneous occurrence of potential minima along the ⟨100⟩ and ⟨110⟩ directions is, however, not possible within the framework of the two-parameter octahedral potential of Eq. (2).

II. MINIMA POSITIONS OF THE TWO-PARAMETER OCTAHEDRAL POTENTIAL

At the extrema positions, both $\partial V/\partial\theta$ and $\partial V/\partial\phi$ should simultaneously vanish. This condition gives the position of the extrema as follows. (i)

$$\begin{aligned}&\theta=0,\pi\ ,\\&\theta=\pi/2,\ \ \phi=0,\pm\pi/2,\pi\ .\end{aligned} \tag{3}$$

These correspond to the six ⟨100⟩ orientational configuration of the impurity. (ii)

$$\theta=\cos^{-1}(1/\sqrt{3}),\quad \phi=\pm\pi/4,\ \pm 3\pi/4\ . \qquad (4)$$
$$\theta=\pi-\cos^{-1}(1/\sqrt{3}),$$

These correspond to the eight ⟨111⟩ orientational configurations. (iii)

$$\theta=\pi/2,\ \phi=\pm\pi/4,\ \pm 3\pi/4\ ,\quad \theta=\pi/4,\ 3\pi/4,\ \phi=0,\ \pm\pi/2,\ \pi\ . \qquad (5)$$

These correspond to the twelve ⟨110⟩ orientational configurations of the impurity.

These are the well-known crystallographic directions, along which the potential extrema have been traditionally sought. The following positions of extrema also exist for restricted sets of values of K and K': (iv)

$$\theta=\cos^{-1}\left[\pm\left[\frac{9}{11}+\frac{20}{231}\frac{K}{K'}\right]^{1/2}\right],\quad \phi=\pm\pi/4,\ \pm 3\pi/4\ . \qquad (6)$$

These directions are coplanar with the corresponding ⟨111⟩ and ⟨110⟩ directions and lie in between them: (v)

$$\theta=\cos^{-1}\left[\pm\left[\frac{1}{11}-\frac{10}{231}\frac{K}{K'}\right]^{1/2}\right],\quad \phi=\pm\pi/4,\ \pm 3\pi/4\ . \qquad (7)$$

These directions are coplanar with the ⟨100⟩ and ⟨111⟩ directions and lie in between them.

The correct condition for minima to occur is that the Jacobian be positive definite as well as $\partial^2V/\partial\theta^2$ and $\partial^2V/\partial\phi^2$. That is,

$$\begin{vmatrix} \frac{\partial^2V}{\partial\theta^2} & \frac{\partial^2V}{\partial\theta\,\partial\phi} \\ \frac{\partial^2V}{\partial\phi\,\partial\theta} & \frac{\partial^2V}{\partial\phi^2} \end{vmatrix} > 0 \qquad (8)$$

and

$$\frac{\partial^2V}{\partial\theta^2}>0,\quad \frac{\partial^2V}{\partial\phi^2}>0\ . \qquad (9)$$

It may be mentioned here that for the first three positions of the extrema mentioned above, we have $\partial^2V/\partial\theta\,\partial\phi=\partial^2V/\partial\phi\,\partial\theta=0$. Hence, the condition given in Eq. (8) for these cases is well contained in Eq. (5) itself. This gives the following conditions for minima to occur:

Along the ⟨100⟩ direction,

$$K>(21/10)K'\ ;$$

Along the ⟨111⟩ direction,

$$K<-(28/5)K'\ ;$$

Along the ⟨110⟩ direction,

$$K<(21/10)K'$$

and

$$K>-(189/20)K'\ .$$

(Both of these conditions are to be simultaneously fulfilled.)

Figure 1 shows the regions for the various potential minima in the K-K' plane. The interesting feature is that for K' positive and

$$-9.45<K/K'<5.6\ ,$$

one gets potential minima simultaneously along the ⟨111⟩ and ⟨110⟩ directions. Similarly, for K' negative and

$$-2.1<K/|K'|<5.6\ ,$$

one gets potential minima simultaneously along the ⟨100⟩ and ⟨111⟩ directions. No such condition is obtained for the occurrence of simultaneous minima along the ⟨100⟩ and ⟨110⟩ directions.

It may be added that the extrema positions, given by (iv) and (v) above, remain valid only for a certain set of values of K and K'. This is restricted for the reason that trigonometric sine and cosine functions have restricted values between $+1$ and -1. It can be quite easily seen that these extrema positions become valid only when we have simultaneous potential minima along the crystallographic directions (the doubly shaded regions in Fig. 1) and that they represent positions of potential maxima.

In Fig. 2, we discuss the situation of the simultaneous occurrence of potential minima along the ⟨111⟩ and ⟨110⟩ directions in somewhat greater detail. Here, K' has to be positive and the ratio K/K' has to be within the limits -5.6 and -9.45. Curve A depicts the relative depth of the two potential minima as a function of K/K' in this limit (i.e., for -5.6 to -9.45). The Y axis represents the minimum potential along ⟨111⟩ direction minus that along ⟨110⟩ direction. So, if this quantity is

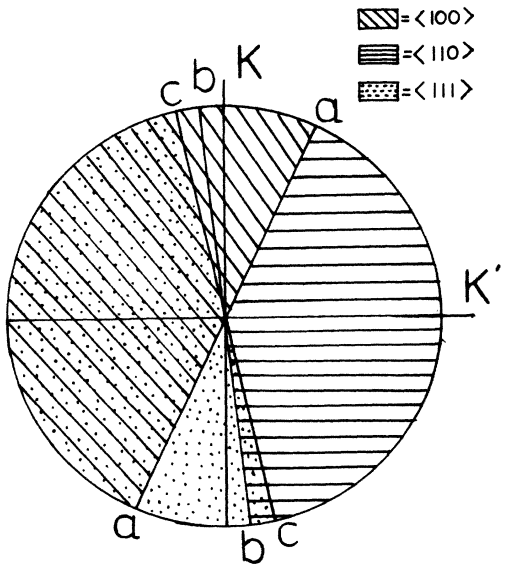

FIG. 1. Regions of potential minima along different crystallographic directions in the K'-K plane. $K/K'=21/10$ for *aa*, $-189/20$ for *bb*, and $-28/5$ for *cc*.

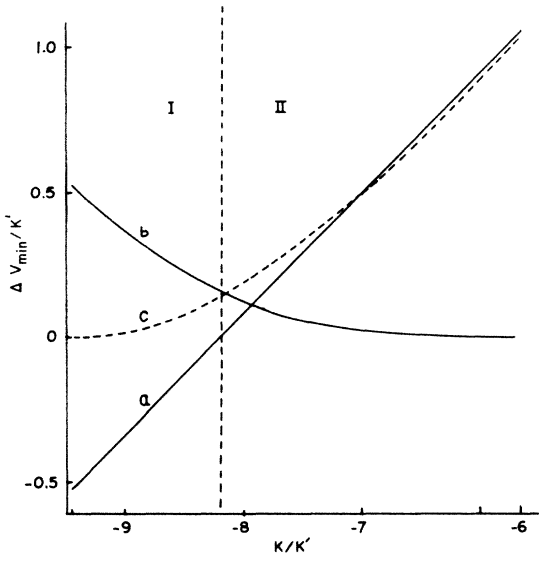

FIG. 2. Illustrations for the case of the simultaneous occurrence of potential minima along the ⟨111⟩ and ⟨110⟩ directions. Curve *a* shows the variation of the relative depth of the two potential minima (ΔV_{min}). Curves *b* and *c* show the variation of the height of the potential barrier for the impurity in the ⟨111⟩ and ⟨110⟩ wells, respectively.

negative, we have deeper minima along the ⟨111⟩ directions, and if this quantity is positive, the reverse becomes the situation. These have been suitably marked as regions I and II, respectively, in the figure. Curve *B* shows the variation of the height of the potential barrier for the impurity lying in the ⟨111⟩ well. The same thing for the impurity lying in the ⟨110⟩ well is shown by curve *C*.

III. LIMITATIONS OF OLD MODELS AND SCOPE OF SIMULTANEOUS POTENTIAL MINIMA IN TWO CRYSTALLOGRAPHIC DIRECTIONS

The possibility of the existence of two sets of minimum-energy orientational configurations of the impurity in the matrix is interesting and exciting from the following point of view. Leaving the ideal case of the KCl-Li^+ system, which exhibits a perfect agreement with the ⟨111⟩ off-centered model of Gomez *et al.*,[9] most of the other paraelectric systems present a difficulty in understanding the various experiments associated with them. Even the minimum-energy orientational configuration of the impurity remains controversial in some of the cases. One example of such a system is the CN^- ion doped in ionic crystals. Initial experiments of Seward and Narayanmurti[3] presented evidence that the impurity could have potential minima along any of the six ⟨100⟩ directions. Then, for the RbCl:CN^- system, paraelectric resonance[10] and specific-heat[11] results at low temperatures revealed the weakness of this model. More recently, careful experiments by Luty[12] and Beyeler[13] on the stress-induced splitting of the intramolecular vibrational line showed that the correct minimum-energy orientational configuration of the CN^- impurity in ionic crystals is along the eight ⟨111⟩ directions. But this could not explain the double bump in the specific-heat results of the RbCl:CN^- system. Even for the KCl:CN^- system, the ⟨111⟩ model works only with limited success. Specifically, certain soft aspects in the tunneling model had to be introduced to understand the stress-induced splitting of the line under large stresses.[13]

Similarly, for the NaBr:F^- system, some controversy exists about its off-centered direction. The calculations of Quigley and Das[14] point toward a deeper minimum along the ⟨111⟩ directions, while the high-field polarization and paraelectric cooling experiments of Rollefson[15] are better fitted by the ⟨110⟩ off-center displacement model. It may be added that even the ⟨110⟩ model could only partially explain the expermental results of Rollefson. For example, the high-field polarization for the electric field parallel to the ⟨111⟩ directions was larger than would be expected for wells only in the ⟨110⟩ directions. As was pointed out by Rollefson[16] later, this suggests the existence of potential minima along the ⟨111⟩ directions also, which are only slightly less deep than the ⟨110⟩ minima. This kind of thing is physically possible even within the framework of the two-parameter potential of Eq. (2), as has been discussed above. Also, the specific-heat anomaly at low temperatures was not consistent within the simple ⟨110⟩ model. In addition to these, the dielectric-constant changes for the system with applied uniaxial stress along the ⟨110⟩ directions is also not consistent with the simple ⟨110⟩ model (see Fig. 15, curve *A*, of Ref. 16).

There are more examples of the systems where simple tunneling models are unable to account for the observed results. The paraelectric resonance experiments on KI:OH^- (Ref. 17) are a suitable example, where backward lines have been observed. We shall focus our attention on the NaBr:F^- and RbCl:CN^- systems only. The other systems with anomalous results may be mentioned somewhere in the course of our discussions.

In light of the present analysis, we can state the following. In cases where the relative values of the K and K' parameters are such that they do not fall within the doubly shaded areas of Fig. 1, we have potential minima along the one crystallographic direction only. This is perhaps the case for systems such as KCl:Li^+ or even KCl:OH^-.

The second situation is one in which the values of the K and K' parameters do fall within the shaded region, so that we have simultaneous potential minima along two crystallographic directions. However, in this limit also, one well could be deeper than the other. In such cases, if the upper well is not sufficiently populated at a given temperature, the system again behaves like an ideal paraelectric system, with potential minima effectively along one crystallographic direction only. However, in experiments where temperature variation of a given physical property is being studied, the situation may become complex. At very low temperatures, when most of the molecules remain in the lower well, the system's behavior can easily be explained in terms of the simple models. At relatively elevated temperatures, more and more molecules are

transferred to the upper well and the system starts showing a marked departure from the ideally expected behavior.

The third interesting situation is one in which both the wells are equally deep. Under such circumstances, the behavior of the system becomes crucially linked to the experimental conditions and one gets controversial results in different experimental circumstances.

IV. THEORY

To see how this double set of potential-minima configurations of the impurity can be helpful in understanding the various anomalous experimental observations, one will have to first work out the appropriate energy eigenvalue problem. Two approaches are mentioned for this in the literature. One is the Devonshire-type calculations,[1,8,18] which start with the free rotor wave functions as the basis set. The properly symmetrized wave functions are then built in accordance with the irreducible representations of the O_h group, and for each irreducible representation, the Hamiltonian matrix is diagonalized to get the energy eigenvalues (and the eigenfunctions). For strong crystal potentials, one better approaches the problem from the opposite extreme, namely, the localized dipole states with orientations along the minima of the crystal potential. These were the six equivalent $\langle 100\rangle$, the eight $\langle 111\rangle$, and the twelve $\langle 110\rangle$ states in the basic paper of Gomez *et al.*[9] In the present case, there is a set each of twelve and eight equivalent states for the case of the simultaneous occurrence of potential minima along the $\langle 111\rangle$ and $\langle 110\rangle$ directions (henceforth this will be labeled case I). Similarly, for the case of the simultaneous occurrence of potential minima along the $\langle 111\rangle$ and $\langle 100\rangle$ directions, we will have to make do with a set each of eight and six equivalent states (henceforth this will be labeled case II).

For case I we take care not to specify too carefully the nature of these states except that they are mutually orthogonal. One of the states in a given group is known, the others are related to it by simple relations. The designation of states has been detailed in Fig. 3.

For a finite crystal field, there will be matrix elements of the Hamiltonian connecting the different states, i.e., there will be a finite probability of tunneling through the potential barrier to a new orientation. There will be equal matrix elements $-\eta$ connecting the states, for example, $|A\rangle$ of the $\langle 111\rangle$ minima group to the nearest-neighboring wells $|B\rangle$, $|D\rangle$, and $|E\rangle$ of the same minima group. Similarly, there will be equal matrix elements $-\eta'$ connecting the states $|a\rangle$ of the $\langle 110\rangle$ minima group to the states $|e\rangle$, $|h\rangle$, $|k\rangle$, and $|n\rangle$ of the same group. We assume that the tunneling matrix elements to the far off wells are insignificant compared to the tunneling matrix elements to the nearest-neighboring wells. Apart from this, the impurity can tunnel from a well of the $\langle 111\rangle$ group to the nearest-neighbor wells of the $\langle 110\rangle$ group. Thus, we have equal matrix elements of the Hamiltonian, say $-\chi$, connecting the states such as $|A\rangle$ of the $\langle 111\rangle$ group to states $|a\rangle$ and $|n\rangle$ of the $\langle 110\rangle$ group. The crystal-field Hamiltonian H_0 can then be written in the form of a 20×20 matrix, as given in Appendix A, where we use yet another parameter p defined as $p=$(depth of well along $\langle 110\rangle$ − depth of well along $\langle 111\rangle$ + ground-state energy of the impurity in the $\langle 110\rangle$ well − ground-state energy of the impurity in the $\langle 111\rangle$ well). p can be either positive or negative depending upon the relative depths of the two sets of wells and the relative ground-state energy of the impurity in the two wells.

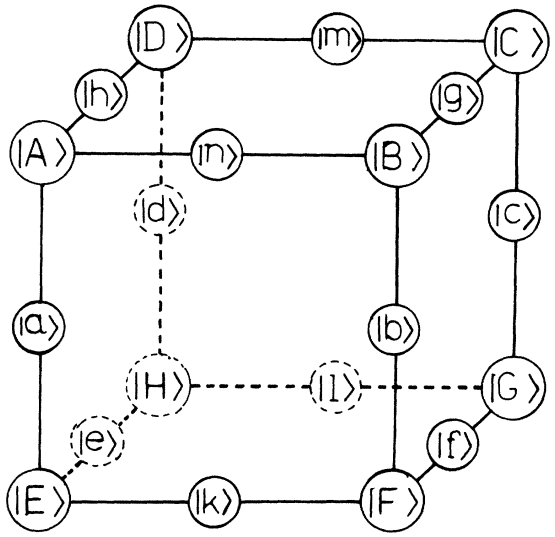

FIG. 3. Pocket states for simultaneous potential minima along the $\langle 111\rangle$ and $\langle 110\rangle$ directions in the O_h symmetry group.

When the wave functions are expressed according to the irreducible representation of the O_h group, the Hamiltonian matrix H_0 is then transformed to $H_0'=u^{\dagger}H_0u$, where u is the proper transformation matrix. Thus, one gets H_0', as given in Appendix B. The wave functions for the twelve $\langle 110\rangle$ wells and the eight $\langle 111\rangle$ wells are given in Tables I and II, respectively.

One can now easily find out the energy eigenvalues of the problem as

$$E(A_{1g}\text{ and }a_{1g})=\frac{p-3\eta-4\eta'}{2}\pm\left[\left[\frac{p-3\eta+4\eta'}{2}\right]^2+6\chi^2\right]^{1/2},$$

$$E(T_{1u}\text{ and }t_{1u})=\frac{p-\eta-2\eta'}{2}\pm\left[\left[\frac{p-\eta+2\eta'}{2}\right]^2+4\chi^2\right]^{1/2},$$

$$E(T_{2g}\text{ and }t_{2g})=\frac{p+\eta}{2}\pm\left[\left[\frac{p+\eta}{2}\right]^2+2\chi^2\right]^{1/2},$$

$$E(A_{2u})=3\eta,\quad E(E_g)=p+2\eta',\quad E(T_{2u})=p+2\eta'.$$

V. DISCUSSION

We now proceed to examine, if the present model can be helpful to our understanding, some of the controversial

TABLE I. Wave functions for the 12 ⟨110⟩ wells.

$$\psi(a_{1g})=\frac{1}{\sqrt{12}}[(a+b+c+d)+(e+f+g+h)+(k+l+m+n)]$$
$$\psi_1(e_g)=\frac{1}{\sqrt{24}}[(a+b+c+d)+(k+l+m+n)-2(e+f+g+h)]$$
$$\psi_2(e_g)=\frac{1}{\sqrt{8}}[(a+b+c+d)-(k+l+m+n)]$$
$$\psi_1(t_{1u})=\frac{1}{\sqrt{8}}[(a+b+k+n)-(c+d+l+m)]$$
$$\psi_2(t_{1u})=\frac{1}{\sqrt{8}}[(a+b+e+h)-(b+c+f+g)]$$
$$\psi_3(t_{1u})=\frac{1}{\sqrt{8}}[(g+h+m+n)-(e+f+k+l)]$$
$$\psi_1(t_{2g})=\tfrac{1}{2}[a+c-b-d]$$
$$\psi_2(t_{2g})=\tfrac{1}{2}[h+f-e-g]$$
$$\psi_3(t_{2g})=\tfrac{1}{2}[n+l-m-k]$$
$$\psi_1(t_{2u})=\frac{1}{\sqrt{8}}[(e+f+n+m)-(h+g+k+l)]$$
$$\psi_2(t_{2u})=\frac{1}{\sqrt{8}}[(b+c+e+h)-(d+a+g+f)]$$
$$\psi_3(t_{2u})=\frac{1}{\sqrt{8}}[(c+d+n+k)-(a+b+m+1)]$$

TABLE II. Wave functions for the eight ⟨111⟩ wells.

$$\psi(A_{1g})=\frac{1}{\sqrt{8}}[A+B+C+D+E+F+G+H]$$
$$\psi_x(T_{1u})=\frac{1}{\sqrt{8}}[(A+B+E+F)-(C+D+G+H)]$$
$$\psi_y(T_{1u})=\frac{1}{\sqrt{8}}[(B+C+F+G)-(A+D+E+F)]$$
$$\psi_z(T_{1u})=\frac{1}{\sqrt{8}}[(A+B+C+D)-(E+F+G+H)]$$
$$\psi_{yz}(T_{2g})=\frac{1}{\sqrt{8}}[(B+C+E+F)-(A+D+F+G)]$$
$$\psi_{zx}(T_{2g})=\frac{1}{\sqrt{8}}[(A+B+G+H)-(C+D+E+F)]$$
$$\psi_{xy}(T_{2g})=\frac{1}{\sqrt{8}}[(B+D+F+H)-(A+C+G+E)]$$
$$\psi(A_{2u})=\frac{1}{\sqrt{8}}[(B+D+E+G)-(A+C+F+H)]$$

results. We limit our discussions to two selected cases: namely, NaBr:F^- and RbCl:CN^-.

A. NaBr:F^- system

While the general features of this system resemble the well-studied case of KCl:Li^+, there are certain remarkable differences as well. First is the field polarization effect. Here the observed polarization was found to be maximum for the applied electric field along the ⟨110⟩ direction, indicating thereby that the F^- ions can be off centered along any of the twelve ⟨110⟩ directions. However, the observed polarization for the ⟨111⟩ field direction was found to be more than that expected from the simple ⟨110⟩ model for the impurity. For the ⟨110⟩ off-centered model, the expression for the polarization is summarized in Table III. The same table also lists the expressions for polarization for the present model of simultaneous minima along the ⟨110⟩ and ⟨111⟩ directions. For the same amount of off-center displacement along the ⟨110⟩ and ⟨111⟩ directions, the saturation polarization for fields along the ⟨110⟩ and ⟨111⟩ directions should be equal (see Table III for the case, $\mu_1=\mu_2$). The larger polarization for the ⟨110⟩ field in this case only indicates that the off-center displacement of the impurity in the ⟨110⟩ minima direction is larger (by about 10 to 12%) than that in the ⟨111⟩ direction. It, however, throws no light on whether the impurity has deeper minima along the ⟨111⟩ or ⟨110⟩ directions.

The second point of difference is the *variation of the dielectric-constant changes* as a function of applied uniaxial stress along the ⟨111⟩ direction (see Fig. 15 of Ref. 16). While Rollefson's observation for the stress along the ⟨100⟩ direction was nicely reproduced by the simple ⟨110⟩ off-centered model for the impurity, the same for the applied stress along the ⟨111⟩ direction could not be as well understood in terms of this model. Table IV summarizes the expected behavior for the simple ⟨110⟩ model and also for the present model. Figure 4 shows the comparison of the experiments with the two models men-

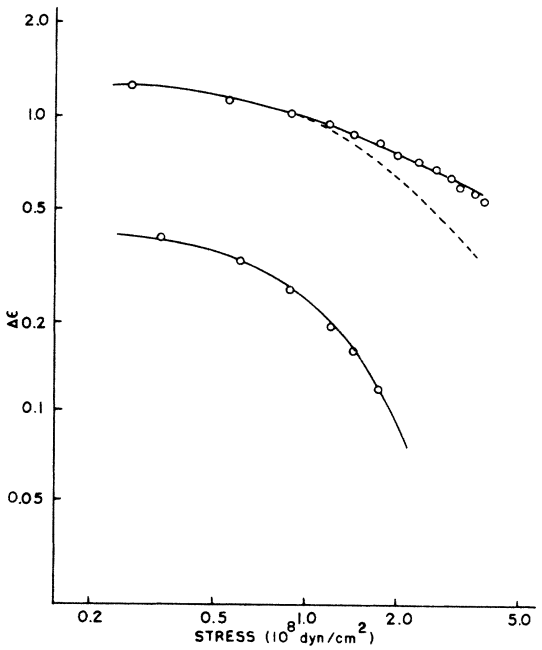

FIG. 4. Variation of dielectric-constant changes as a function of applied uniaxial stress along the ⟨111⟩ direction for the NaBr:F^- system. Open circles are experimental points of Rollefson (Ref. 16); the dashed curve is the calculated results of Rollefson for the ⟨110⟩ off-centered model for impurity. Solid curves depict calculated results on the basis of the present work. [All curves are plotted for a frequency of 0.1 kHz and a F^--ion concentration of 5.1×10^{18} cm^{-3} (top curve) and 1.8×10^{18} cm^{-3} (bottom curve).]

TABLE III. Expressions for polarization for the simple ⟨110⟩ off-centered model and the present model of simultaneous potential minima along the ⟨110⟩ and ⟨111⟩ directions. Here, $x=\mu E/kT$ and the asterisk denotes expressions which represent the saturation value for the case $x \gg 1$ (i.e., for large field).

Direction of applied electric field	Polarization as expected from the simple ⟨110⟩ model	Polarization as expected from present model
⟨100⟩	$P=\frac{N\mu}{\sqrt{2}}\frac{e^{x/\sqrt{2}}-e^{-x/\sqrt{2}}}{1+e^{x/\sqrt{2}}+e^{-x/\sqrt{2}}}$	$P=N\frac{\mu_1/\sqrt{2}(e^{x_1/\sqrt{2}}-e^{-x_1/\sqrt{2}})+\mu_2/\sqrt{3}(e^{x_2/\sqrt{3}}-e^{-x_2/\sqrt{3}})}{1+(e^{x_1/\sqrt{2}}+e^{-x_1/\sqrt{2}})+(e^{x_2/\sqrt{3}}+e^{-x_2/\sqrt{3}})}$
	$P=\frac{N\mu}{2}$ *	$P=\frac{N\mu'}{2}$ *
⟨111⟩	$P=\sqrt{2/3}N\mu\frac{e^{2x/\sqrt{6}}-e^{-2x/\sqrt{6}}}{2+e^{2x/\sqrt{6}}+e^{-2x/\sqrt{6}}}$	$P=N\frac{\sqrt{6}\mu_1(e^{2x_1/\sqrt{6}}-e^{-2x_1/\sqrt{6}})+\mu_2(e^{x_2}-e^{-x_2}+e^{x_2/3}-e^{-x_2/3})}{6+3(e^{2x_1/\sqrt{6}}+e^{-2x_1/\sqrt{6}})+(e^{x_2}+e^{-x_2})+(e^{x_2/3}+e^{-x_2/3})}$
	$P=\sqrt{2/3}N\mu$ *	$P=N\mu_2$ *
⟨110⟩	$P=N\mu\frac{(e^x-e^{-x})+2(e^{x/2}-e^{-x/2})}{2+(e^x+e^{-x})+4(e^{x/2}+e^{-x/2})}$	$P=N\frac{\mu_1[(e^{x_1}-e^{-x_1})+2(e^{x_1/2}-e^{-x_1/2})]+(4/\sqrt{6})\mu_2(e^{2x_2/\sqrt{6}}-e^{-2x_2/\sqrt{6}})}{6+(e^{x_1}+e^{-x_1})+4(e^{x_1/2}+e^{-x_1/2})+2(e^{2x_2/\sqrt{6}}+e^{-2x_2/\sqrt{6}})}$
	$P=N\mu$ *	$P=N\mu_1$ *

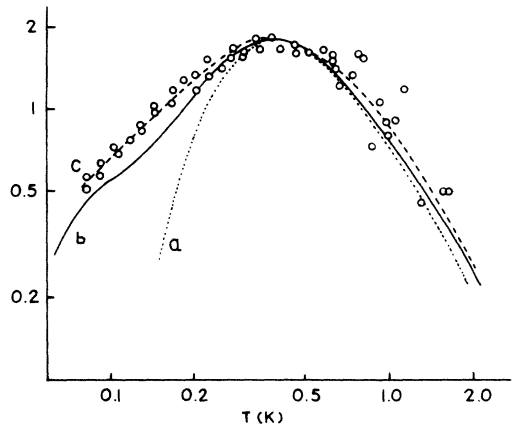

FIG. 5. Variation of specific heat versus temperature for the NaBr:F^- system. Curve *b* is obtained on the basis of the proposed model, while curve *a* is for the simple ⟨110⟩ model and curve *c* is for Rollefson's random internal stress model.

tioned above. One can easily see that the present model of simultaneous potential minima along the ⟨111⟩ and ⟨110⟩ directions makes for a better understanding of this experiment. It may be added here that a ⟨111⟩ off-centered impurity model gives zero stress energy for the applied stress along the ⟨100⟩ direction. This is, perhaps,

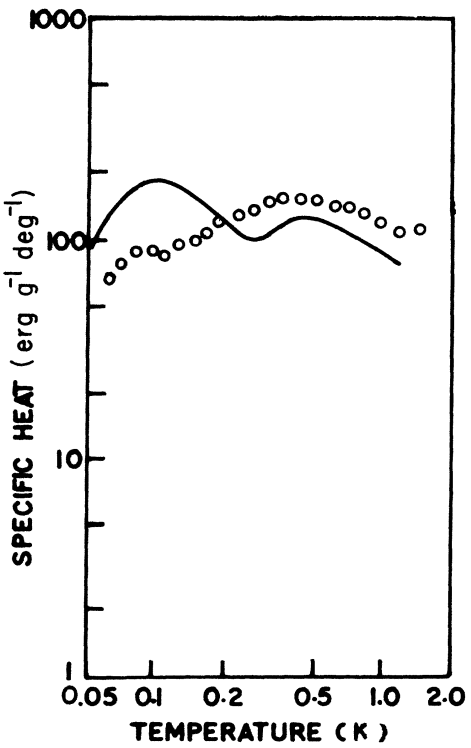

FIG. 6. Variation of specific heat with temperature for the RbCl:CN^- system; open circles are experimental points (Ref. 11) and the solid curve shows calculated results on the basis of the present model.

TABLE IV. Expression for the dipole contribution to the dielectric constant as a function of stress for the simple ⟨110⟩ model and the present model.

Direction of applied uniaxial stress	Dipole contribution to the dielectric constant: For the simple ⟨110⟩ model	For the present model
⟨100⟩	$\frac{N_F\mu^2}{3kT}\frac{3}{e^{\Delta/kT}+2}$	$\frac{N_F\mu_1^2}{3kT}\frac{3+2(\mu_2/\mu_1)^2e^{\Delta/3kT}e^{-p/kT}}{2+e^{\Delta/kT}+2e^{\Delta/3kT}e^{-p/kT}}$
⟨111⟩	$\frac{N_F\mu^2}{3kT}\frac{2}{e^{\Delta/kT}+1}$	$\frac{N_F\mu_1^2}{3kT}\frac{6+(\mu_2/\mu_1)^2(3e^{(\Delta-\Delta')/kT}+e^{(\Delta+\Delta'/3)/kT})e^{-p/kT}}{3+3e^{\Delta/kT}+(e^{(\Delta-\Delta')/kT}+3e^{(\Delta+\Delta'/3)/kT})e^{-p/kT}}$

the reason why the simple ⟨110⟩ model could correctly explain the experimental results for this direction of the applied stress. The ⟨111⟩ off-centered system *does* have nonzero stress energy for the applied stress along the ⟨111⟩ direction. Hence, for this stress direction the presence of additional potential minima along the ⟨111⟩ directions *does* affect the results. When this is properly taken into account, we get a better explanation of the experimental results.

The third and the most important difference is the observed specific-heat results at low temperatures. It shows a peak at about 0.5 K, indicating the existence of tunneling levels at about that energy (on the temperature scale), but the specific-heat does not drop exponentially at the lower-temperature side of the peak, as is expected from the simple tunneling model (the Schottky anomaly). The result for the present model with $\chi=0$, $\eta=\eta'$, and $p=-0.6\eta$ is shown by curve *b* in Fig. 5, where experimental points have also been plotted for ready comparison. One can see that there is improved agreement with the experiment, as compared to the expected Schottky anomaly associated with the simple ⟨110⟩ model of the impurity (curve *a*). However, one has a slightly worse agreement than with the random internal stress model of Rollefson (curve *c*).

This does not undermine the importance of the present model, for it is somewhat hard to believe that, while the internal random stress of the crystal affects so severely the results for the NaBr:F^- system, it does not show any effect at all in the KCl:Li^+ system. It is easier to believe that the small discrepancy between the observed data and the results of the present model is due to the presence of the internal stress.

B. RbCl:CN^- system: Specific-heat anomaly

The RbCl:CN^- system is not very well understood in terms of the existing models. There happen to be controversies and unexplained results in almost all the experiments performed on this system. First, the specific heat at low temperatures showed double peaks, which is a characteristic feature of this system. Second, the paraelectric resonance experiments by Dreyfus[10] showed anomalous results.

In the present communication, we have not discussed the effect of electric and stress fields on the tunneling states of the two-potential model impurities. Hence, we postpone the discussion of anomalous paraelectric resonance experiments to a later communication. Here, we shall limit ourselves to the discussion of the specific-heat anomaly only.

The specific-heat anomaly in the case of the RbCl:CN^- system was explained by Pompi and Narayanamurti[19,20] by adding a small tetragonal deformation term to the Devonshire potential, which was brought in to account for the surprising behavior of the electric-field-induced dichroism of the CN^- ion in alkali halides. The result of their measurement was that the absorption coefficient decreased with field for parallel polarization. The tetragonal deformation in the Devonshire potential could explain to some extent the opposite sign of the electro-optical effect. However, in light of careful measurements by Luty,[12] in which the reported electro-optical effect of opposite sign was not obtained, the validity of introducing a tetragonal deformation in the Devonshire potential becomes doubtful.

In the framework of the proposed model, we have already discussed the energy-level structure for impurities having two sets of potential-minima configurations (see Sec. IV). With $p=2$ GHz, $\eta=0.6$ GHz, $\eta'=0.9$ GHz, and $\chi=7$ GHz, we get a calculated Schottky anomaly, as shown by the continuous curve in Fig. 6. The double peaks at the proper positions are very well obtained. However, the peak obtained at higher temperature is weaker than that at the lower temperature, which is opposite of what has been experimentally observed. For the moment, we are not in a position to comment on this discrepancy. Perhaps it is the effect of the residual NCO^- impurities in the crystal, but this fact will have to be experimentally verified.

ACKNOWLEDGMENTS

We are thankful to Dr. V. K. Agrawal for helpful discussions. Thanks are also due to Council for Scientific and Industrial Research (India) and University Grants Commission (India) for financial assistance.

APPENDIX A

In Eq. (A1) we show the crystal-field Hamiltonian written as a 20×20 matrix.

APPENDIX B

In Eq. (B1) we show the transformed 20×20 Hamiltonian matrix.

$$
H_0 = \begin{array}{c|cccccccccccccccccccccccccc}
 & |A\rangle & |B\rangle & |C\rangle & |D\rangle & |E\rangle & |F\rangle & |G\rangle & |H\rangle & |a\rangle & |b\rangle & |c\rangle & |d\rangle & |e\rangle & |f\rangle & |g\rangle & |h\rangle & |k\rangle & |l\rangle & |m\rangle & |n\rangle \\
\hline
\langle A| & 0 & -\eta & 0 & -\eta & -\eta & 0 & 0 & 0 & -\chi & 0 & 0 & 0 & 0 & 0 & 0 & -\chi & 0 & 0 & 0 & -\chi \\
\langle B| & -\eta & 0 & -\eta & 0 & 0 & -\eta & 0 & 0 & 0 & -\chi & 0 & 0 & 0 & 0 & 0 & 0 & 0 & 0 & 0 & -\chi \\
\langle C| & 0 & -\eta & 0 & -\eta & 0 & 0 & -\eta & -\chi & -\eta' & 0 & -\eta' & -\eta' & 0 & 0 & -\chi & 0 & 0 & 0 & -\chi & 0 \\
\langle D| & -\eta & 0 & -\eta & 0 & 0 & 0 & 0 & -\chi & -\eta' & 0 & -\eta' & -\eta' & 0 & 0 & -\chi & 0 & 0 & 0 & -\chi & 0 \\
\langle E| & -\eta & 0 & -\eta & 0 & 0 & -\eta & -\eta & 0 & 0 & 0 & 0 & 0 & -\chi & 0 & 0 & -\chi & 0 & 0 & 0 & 0 \\
\langle F| & 0 & 0 & 0 & 0 & -\eta & 0 & -\eta & -\eta & 0 & 0 & 0 & -\chi & -\chi & -\chi & 0 & 0 & -\chi & 0 & 0 & 0 \\
\langle G| & -\chi & 0 & -\chi & -\eta & -\chi & -\chi & 0 & 0 & 0 & -\chi & 0 & 0 & -\eta' & 0 & 0 & -\eta' & -\eta' & -\eta' & 0 & -\eta' \\
\langle H| & 0 & -\chi & 0 & 0 & 0 & -\chi & 0 & 0 & 0 & -\chi & 0 & 0 & -\eta' & 0 & 0 & -\eta' & -\eta' & -\eta' & 0 & -\eta' \\
\langle a| & 0 & 0 & 0 & 0 & 0 & 0 & 0 & 0 & 0 & 0 & 0 & 0 & 0 & 0 & 0 & 0 & 0 & 0 & 0 & 0 \\
\langle b| & 0 & 0 & 0 & 0 & 0 & 0 & 0 & 0 & 0 & 0 & 0 & 0 & 0 & 0 & 0 & 0 & 0 & 0 & 0 & 0 \\
\langle c| & 0 & 0 & 0 & 0 & 0 & 0 & 0 & 0 & 0 & 0 & 0 & 0 & 0 & 0 & 0 & 0 & 0 & 0 & 0 & 0 \\
\langle d| & 0 & 0 & 0 & 0 & 0 & 0 & 0 & 0 & 0 & 0 & 0 & 0 & 0 & 0 & 0 & 0 & 0 & 0 & 0 & 0 \\
\langle e| & 0 & 0 & 0 & 0 & 0 & 0 & 0 & 0 & 0 & 0 & 0 & 0 & 0 & 0 & 0 & 0 & 0 & 0 & 0 & 0 \\
\langle f| & 0 & 0 & 0 & 0 & 0 & 0 & 0 & 0 & 0 & 0 & 0 & 0 & 0 & 0 & 0 & 0 & 0 & 0 & 0 & 0 \\
\langle g| & 0 & 0 & 0 & 0 & 0 & 0 & 0 & 0 & 0 & 0 & 0 & 0 & 0 & 0 & 0 & 0 & 0 & 0 & 0 & 0 \\
\langle h| & -\chi & 0 & 0 & 0 & 0 & 0 & 0 & 0 & 0 & 0 & 0 & 0 & 0 & 0 & 0 & 0 & 0 & 0 & 0 & 0 \\
\langle k| & 0 & 0 & 0 & 0 & 0 & 0 & 0 & 0 & 0 & 0 & 0 & 0 & 0 & 0 & 0 & 0 & 0 & 0 & 0 & 0 \\
\langle l| & 0 & 0 & 0 & 0 & 0 & 0 & 0 & 0 & 0 & 0 & 0 & 0 & 0 & 0 & 0 & 0 & 0 & 0 & 0 & 0 \\
\langle m| & 0 & 0 & 0 & 0 & 0 & 0 & 0 & 0 & 0 & 0 & 0 & 0 & 0 & 0 & 0 & 0 & 0 & 0 & 0 & 0 \\
\langle n| & -\chi & -\chi & 0 & 0 & 0 & 0 & 0 & 0 & 0 & 0 & 0 & 0 & 0 & 0 & 0 & 0 & 0 & 0 & 0 & 0
\end{array}
\qquad \text{(A1)}
$$

$$H_0' =$$

A_{1g}	T_{1u}	T_{1u}	T_{1u}	T_{2g}	T_{2g}	T_{2g}	A_{2u}	a_{1g}	t_{1u}	t_{1u}	t_{1u}	t_{2g}	t_{2g}	t_{2g}	t_{2u}	t_{2u}	t_{2u}	e_g	e_g	e_g
-3η	0	0	0	0	0	0	0	$-\sqrt{6}\chi$	0	0	0	0	0	0	0	0	0	0	0	0
0	$-\eta$	0	0	0	0	0	0	0	-2χ	0	0	0	0	0	0	0	0	0	0	0
0	0	$-\eta$	0	0	0	0	0	0	0	-2χ	0	0	0	0	0	0	0	0	0	0
0	0	0	$-\eta$	0	0	0	0	0	0	0	-2χ	0	0	0	0	0	0	0	0	0
0	0	0	0	η	0	0	0	0	0	0	0	$-\sqrt{2}\chi$	0	0	0	0	0	0	0	0
0	0	0	0	0	η	0	0	0	0	0	0	0	$-\sqrt{2}\chi$	0	0	0	0	0	0	0
0	0	0	0	0	0	η	0	0	0	0	0	0	0	$-\sqrt{2}\chi$	0	0	0	0	0	0
0	0	0	0	0	0	0	3η	0	0	0	0	0	0	0	0	0	0	0	0	0
$-\sqrt{6}\chi$	0	0	0	0	0	0	0	$p-4\eta'$	0	0	0	0	0	0	0	0	0	0	0	0
0	-2χ	0	0	0	0	0	0	0	$p-2\eta'$	0	0	0	0	0	0	0	0	0	0	0
0	0	-2χ	0	0	0	0	0	0	0	$p-2\eta'$	0	0	0	0	0	0	0	0	0	0
0	0	0	-2χ	0	0	0	0	0	0	0	$p-2\eta'$	0	0	0	0	0	0	0	0	0
0	0	0	0	$-\sqrt{2}\chi$	0	0	0	0	0	0	0	p	0	0	0	0	0	0	0	0
0	0	0	0	0	$-\sqrt{2}\chi$	0	0	0	0	0	0	0	p	0	0	0	0	0	0	0
0	0	0	0	0	0	$-\sqrt{2}\chi$	0	0	0	0	0	0	0	p	0	0	0	0	0	0
0	0	0	0	0	0	0	0	0	0	0	0	0	0	0	$p+2\eta'$	0	0	0	0	0
0	0	0	0	0	0	0	0	0	0	0	0	0	0	0	0	$p+2\eta'$	0	0	0	0
0	0	0	0	0	0	0	0	0	0	0	0	0	0	0	0	0	$p+2\eta'$	0	0	0
0	0	0	0	0	0	0	0	0	0	0	0	0	0	0	0	0	0	$p+2\eta'$	0	0
0	0	0	0	0	0	0	0	0	0	0	0	0	0	0	0	0	0	0	$p+2\eta'$	0
0	0	0	0	0	0	0	0	0	0	0	0	0	0	0	0	0	0	0	0	$p+2\eta'$

(B1)

[1]A. F. Devonshire, Proc. R. Soc. London, Ser. A **153**, 601 (1936).
[2]W. N. Lawless, J. Phys. Chem. Solids **28**, 1755 (1967).
[3]W. D. Seward and V. Narayanamurti, Phys. Rev. **148**, 463 (1966).
[4]W. H. Flygare, J. Chem. Phys. **39**, 2263 (1963).
[5]D. E. Mann, N. Acquista, and D. White, J. Chem. Phys. **44**, 3453 (1966).
[6]D. N. Mitra, V. K. Agrawal, and G. K. Pandey, Solid State Commun. **8**, 1645 (1970).
[7]Note that the ratio mentioned here is different from that mentioned in Ref. 6. This is because the K and K' parameters of Ref. 6 are not the same as those defined here. A proper transformation for the two sets of potential parameters has been derived in the footnote of Ref. 8.
[8]H. U. Beyeler, Phys. Status Solidi B **53**, 419 (1972).
[9]M. Gomez, S. P. Bowen, and Z. A. Krumhansl, Phys. Rev. **153**, 1009 (1967).
[10]R. W. Dreyfus, J. Phys. Chem. Solids **29**, 1941 (1968).
[11]J. P. Harrison, P. P. Peressini, and R. O. Pohl, Phys. Rev. **167**, 856 (1968).
[12]F. Luty, Phys. Rev. B **10**, 3677 (1974).
[13]H. U. Beyeler, Phys. Rev. B **11**, 3078 (1975).
[14]R. J. Quigley and T. P. Das, Phys. Rev. B **7**, 4004 (1973).
[15]R. J. Rollefson, Phys. Rev. B **5**, 3235 (1972).
[16]R. J. Rollefson, Phys. Rev. B **7**, 4006 (1973).
[17]F. Bridges, Solid State Commun. **13**, 1877 (1973).
[18]P. Sauer, Z. Phys. **194**, 360 (1966).
[19]R. L. Pompi and V. Narayanamurti, Solid State Commun. **6**, 645 (1968).
[20]V. Narayanamurti and R. O. Pohl, Rev. Mod. Phys. **42**, 201 (1970).